

# Enhancement of optics-to-THz conversion efficiency by metallic slot waveguides

Zhichao Ruan<sup>1,2,†</sup>, Georgios Veronis<sup>3</sup>, Konstantin L. Vodopyanov<sup>1</sup>,  
Marty M. Fejer<sup>1</sup> and Shanhui Fan<sup>1,2,‡</sup>

<sup>1</sup>Ginzton Laboratory, Stanford University, Stanford, California 94305

<sup>2</sup>Department of Electrical Engineering, Stanford University, Stanford, California 94305

<sup>3</sup>Department of Electrical and Computer Engineering and Center for Computation and Technology, Louisiana State University, Baton Rouge, Louisiana 70803

<sup>†</sup>[zhichao@stanford.edu](mailto:zhichao@stanford.edu) <sup>‡</sup>[shanhui@stanford.edu](mailto:shanhui@stanford.edu)

**Abstract:** A metallic slot waveguide, with a dielectric strip embedded within, is investigated for the purpose of enhancing the optics-to-THz conversion efficiency using the difference-frequency generation (DFG) process. To describe the frequency conversion process in such lossy waveguides, a fully-vectorial coupled-mode theory is developed. Using the coupled-mode theory, we outline the basic theoretical requirements for efficient frequency conversion, which include the needs to achieve large coupling coefficients, phase matching, and low propagation loss for both the optical and THz waves. Following these requirements, a metallic waveguide is designed by considering the trade-off between modal confinement and propagation loss. Our numerical calculation shows that the conversion efficiency in these waveguide structures can be more than one order of magnitude larger than what has been achieved using dielectric waveguides. Based on the distinct impact of the slot width on the optical and THz modal dispersion, we propose a two-step method to realize the phase matching for general pump wavelengths.

© 2009 Optical Society of America

**OCIS codes:** (190.4390) Nonlinear optics, integrated optics; (230.7370) Waveguides; (240.6680) Surface plasmons;

---

## References and links

1. M. Tonouchi, "Cutting-edge terahertz technology," *Nature Photonics* **1**, 97 (2007).
2. Y. R. Shen, *The principles of nonlinear optics* (New York, Wiley-Interscience, 1984).
3. R. W. Boyd, *Nonlinear Optics* (Academic Press, 2003).
4. Y. Jiang and Y. J. Ding, "Efficient terahertz generation from two collinearly propagating CO<sub>2</sub> laser pulses," *Appl. Phys. Lett.* **91**, 091108 (2007).
5. D. E. Thompson and P. D. Coleman, "Step-Tunable Far Infrared Radiation by Phase Matched Mixing in Planar-Dielectric Waveguides," *IEEE Trans. Microwave Theory Tech.* **22**, 995–1000 (1974).
6. W. Shi and Y. J. Ding, "Designs of terahertz waveguides for efficient parametric terahertz generation," *Appl. Phys. Lett.* **82**, 4435 (2003).
7. H. Cao, R. A. Linke, and A. Nahata, "Broadband generation of terahertz radiation in a waveguide," *Opt. Lett.* **29**, 1751–1753 (2004).
8. V. Berger and C. Sirtori, "Nonlinear phase matching in THz semiconductor waveguides," *Semicond. Sci. Technol.* **19**, 964–970 (2004).
9. A. C. Chiang, T. D. Wang, Y. Y. Lin, S. T. Lin, H. H. Lee, Y. C. Huang, and Y. H. Chen, "Enhanced terahertz-wave parametric generation and oscillation in lithium niobate waveguides at terahertz frequencies," *Opt. Lett.* **30**, 3392–3394 (2005).

10. Y. Takushima, S. Y. Shin, and Y. C. Chung, "Design of a LiNbO<sub>3</sub> ribbon waveguide for efficient difference-frequency generation of terahertz wave in the collinear configuration," *Opt. Express* **15**, 14783–14792 (2007).
11. C. Staus, T. Kuech, and L. McCaughan, "Continuously phase-matched terahertz difference frequency generation in an embedded-waveguide structure supporting only fundamental modes," *Opt. Express* **16**, 13296–13303 (2008).
12. K. L. Vodopyanov and Y. H. Avetisyan, "Optical terahertz wave generation in a planar GaAs waveguide," *Opt. Lett.* **33**, 2314–2316 (2008).
13. A. Marandi, T. E. Darcie, and P. P. M. So, "Design of a continuous-wave tunable terahertz source using waveguide-phase-matched GaAs," *Opt. Express* **16**, 10427–10433 (2008).
14. S. S. Dhillon, C. Sirtori, J. Alton, S. Barbieri, A. de Rossi, H. E. Beere and D. A. Ritchie, "Terahertz transfer onto a telecom optical carrier," *Nature Photonics* **1**, 411–415 (2007).
15. E. R. Brown, K. A. McIntosh, K. B. Nichols, and C. L. Dennis, "Photomixing up to 3.8 THz in low-temperature-grown GaAs," *Appl. Phys. Lett.* **66**, 285, (1995).
16. A. Snyder and J. Love, *Optical waveguide theory* (Kluwer Academic Pub, 1983).
17. P. R. Villeneuve, S. Fan, J. D. Joannopoulos, K. Y. Lim, G. S. Petrich, L. A. Kolodziejski, and R. Reif, "Air-bridge microcavities," *Appl. Phys. Lett.* **67**, 167 (1995).
18. K. L. Vodopyanov, M. M. Fejer, X. Yu, J. S. Harris, Y. S. Lee, W. C. Hurlbut, V. G. Kozlov, D. Bliss, and C. Lynch, "Terahertz-wave generation in quasi-phase-matched GaAs," *Appl. Phys. Lett.* **89**, 141,119 (2006).
19. I. Mehdì, S. C. Martin, R. J. Dengler, R. P. Smith, and P. H. Siegel, "Fabrication and performance of planar Schottky diodes with T-gate-like anodes in 200-GHz subharmonically pumped waveguide mixers," *IEEE Microwave and Guided Wave Lett.* **6**, 49–51 (1996)
20. S. M. Marazita, W. L. Bishop, J. L. Hesler, K. Hui, W. E. Bowen, T. W. Crowe, V. M. W. Inc, and V. A. Charlottesvile, "Integrated GaAs Schottky mixers by spin-on-dielectric wafer bonding," *IEEE Trans. Electron Devices* **47**, 1152–1157 (2000)
21. P. H. Siegel, R. P. Smith, M. C. Graidis, and S. C. Martin, "2.5-THz GaAs monolithic membrane-diode mixer," *IEEE Trans. Microwave Theory Tech.* **47**, 596–604 (1999)
22. K. Aoki, H. T. Miyazaki, H. Hirayama, K. Inoshita, T. Baba, K. Sakoda, N. Shinya, and Y. Aoyagi, "Microassembly of semiconductor three-dimensional photonic crystals," *Nature Materials* **2**, 117–121 (2003).
23. E. E. Russell and E. Bell, "Measurement of the Optical Constants of Crystal Quartz in the Far Infrared with the Asymmetric Fourier-Transform Method," *J. Opt. Soc. Am.* **57**, 341–348 (1967).
24. D. Grischkowsky, S. Keiding, M. van Exter, and C. Fattinger, "Far-infrared time-domain spectroscopy with terahertz beams of dielectrics and semiconductors," *J. Opt. Soc. Am. B* **7**, 2006–2015 (1990).
25. M. Ordal, L. Long, R. Bell, S. Bell, R. Bell, and R. Alexander, "Optical properties of the metals Al, Co, Cu, Au, Fe, Pb, Ni, Pd, Pt, Ag, Ti, and W in the infrared and far infrared," *Appl. Opt.* **22**, 1099–1119 (1983).
26. E. D. Palik, *Handbook of Optical Constants in Solids*, vol. 1 (Academic Press, Boston, 1991).
27. K. Vodopyanov, "Optical THz-wave generation with periodically-inverted GaAs," *Laser and Photonics Reviews* **2**, 11 (2008).
28. W. C. Hurlbut, Y. S. Lee, K. L. Vodopyanov, P. S. Kuo, and M. M. Fejer, "Multiphoton absorption and nonlinear refraction of GaAs in the mid-infrared," *Opt. Lett.* **32**, 668–670 (2007).
29. P. Bienstman, "Rigorous and efficient modelling of wavelength scale photonic components," Universiteit Gent Thesis (2001).

---

## 1. Introduction

Many important applications of THz radiation [1] demand coherent THz sources. Among all techniques to generate coherent THz radiation, the difference frequency generation (DFG) process is of importance because it offers the advantages of relative compactness, straightforward alignment, and room-temperature working environment. In difference frequency generation, two optical pump beams, with their frequencies separated by a few THz, interact through a  $\chi^{(2)}$  process to generate a THz beam. In general, the conversion efficiency of DFG is proportional to the intensities of the pump beams [2, 3]. Consequently, in bulk crystals, it is desirable to use a beam with a small radius. On the other hand, an excessively small beam radius can result in strong diffraction effects. As a result, there exists an optimal beam radius. In a bulk GaSe nonlinear crystal, for example, when generating 0.914 THz wave from the mixing of two CO<sub>2</sub> lasers near 10  $\mu\text{m}$ , the maximum efficiency of  $3.9 \times 10^{-9} \text{ W}^{-1}$  occurs at an optimal optical beam radius of 10.59  $\mu\text{m}$  [4].

It has long been recognized that further efficiency gain can be achieved with the use of waveguide devices. In a waveguide, a tightly confined beam can propagate over long distance

without suffering from diffraction effect [5, 6, 7, 8, 9, 10, 11, 12, 13]. Indeed, when using the DFG process for THz generation, the highest efficiency reported to date [11] was accomplished using a dielectric waveguide geometry. In applying dielectric waveguides to THz generation, however, a unique challenge is the very large wavelength differences between the optical and the THz waves. In a dielectric waveguide structure, the strongest confinement of an electromagnetic wave typically occurs when the waveguide dimension is comparable to the wavelength. Thus, a micron-scale dielectric waveguide, which is optimal for optical waveguiding, provides only weak confinement of the THz wave. On the other hand, a single-mode strongly-confining dielectric guide for THz wave would have a dimension of hundreds of microns. For an optical wave such a guide is highly multi-moded, and has very limited modal confinement. As a result, in a dielectric waveguide geometry, as well as in some of the planar waveguide structures utilizing metal plates (e.g. the geometry in Ref. [14]), the modal overlap of THz and optical modes are far from ideal for the DFG processes.

To overcome the limitation of such waveguides, in this paper we analyze in detail the use of metallic slot waveguide for THz generation purposes. The basic geometry, as shown in Fig. 1, consists of a dielectric strip made of a nonlinear crystal embedded in a metallic slot waveguide. The dielectric strip, with the cross-section dimension in the micron scale, is designed to provide single-mode guiding and strong modal confinement of the optical wave. The use of a metallic slot, on the other hand, allows deep sub-wavelength confinement of the THz wave. As a result, the modal overlap of optical and THz waves is greatly improved in this geometry, which results in greatly enhanced conversion efficiency. Our analysis indicates that more than an order of magnitude improvement in conversion efficiency is achievable compared with state-of-the-art dielectric waveguide results [11]. We note that although a low-temperature-grown GaAs photomixer [15] achieved a comparable conversion efficiency to that of our design at  $< 2$  THz, the photomixer suffers from dramatic efficiency roll-off starting at around 0.5 THz (where terahertz power scales as the fourth power of the inverse frequency), due to finite carrier lifetime of GaAs. Hence photomixers could not efficiently produce high power at frequencies  $> 2$  THz, whereas in our design there is no such limitation. Another advantage of the DFG process is power scalability: unlike photomixers, nonlinear optical sources do not suffer from saturation of THz output power and typically show quadratic dependence vs. pump power.

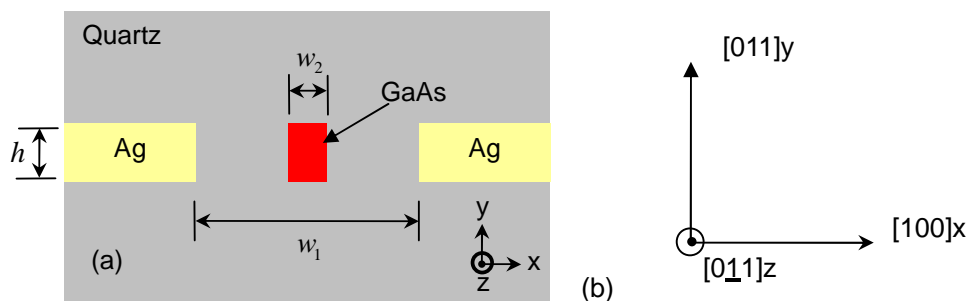


Fig. 1. (a) Schematic of the metal slot waveguide integrated with an embedded GaAs strip: The background is quartz, the silver film and the GaAs strip have the same thickness  $h$ , and the width of the slot and the GaAs strip are  $w_1$  and  $w_2$ , respectively. (b) Orientation of the embedded GaAs.

The use of metal, in general, induces loss as well as substantial waveguide dispersion at both THz and optical wavelengths. The design of an optimal waveguide geometry thus involves a careful consideration of many competing requirements. Our work is therefore substantially different from a closely related recent paper [13], where THz wavelength conversion using

a metal waveguide was first discussed. In Ref. [13], the material loss due to metal and the impact of the waveguide geometry on the dispersive properties are not considered. Our analysis indicates that these effects, ignored in [13], in fact can be very substantial in metallic waveguide geometries.

The paper is organized as follows: In Section 2, we outline the basic theoretical requirement for efficient frequency conversion using coupled-mode theory. In Section 3, we present an example of a metallic waveguide structure designed to have a high conversion efficiency when pumped at about 2  $\mu\text{m}$  wavelength. In Section 4, we discuss in detail many of the considerations that lead to the design in Section 3. Finally, in Section 5, we propose a general method for designing such waveguides at different pump wavelengths.

## 2. Theory

We start by outlining the basic theoretical requirement for efficient frequency conversion. For this purpose, we use a form of coupled-mode theory that is fully vectorial, and is developed specifically for waveguides with substantial loss.

Consider the DFG process in a waveguide where two optical beams at frequencies  $\omega_2$  and  $\omega_3$  mix to produce a THz beam at  $\omega_1 = \omega_3 - \omega_2$ . For each frequency  $\omega_j$ , we assume that the corresponding electromagnetic fields  $\{\mathbf{E}_j, \mathbf{H}_j\}$  are in a single mode that propagates along the  $+z$  direction, and can be written in the following form:

$$\begin{aligned}\mathbf{E}_j &= A_j(z) (\mathbf{e}_{j,t} + \mathbf{e}_{j,z}) \exp(i\beta_j z) \\ \mathbf{H}_j &= A_j(z) (\mathbf{h}_{j,t} + \mathbf{h}_{j,z}) \exp(i\beta_j z).\end{aligned}\quad (1)$$

Here,  $\beta_j$  is the real part of the wave number,  $A_j$  is the mode amplitude, and  $\{\mathbf{e}_{j,t(z)}, \mathbf{h}_{j,t(z)}\}$  are the modal profiles, with the subscripts  $t$  and  $z$  representing the transverse and longitudinal components, respectively. The modal profile is normalized such that

$$\int d\sigma \cdot \frac{1}{2} (\mathbf{e}_{j,t} \times \mathbf{h}_{j,t}) = 1, \quad (2)$$

where the integration occurs over the entire waveguide cross-section, and  $d\sigma$  is a vector along the  $z$ -direction. With such normalization, the  $\mathbf{e}$  and  $\mathbf{h}$  in the modal profile have units of  $\text{V}/(\text{m}\sqrt{\text{W}})$  and  $\text{A}/(\text{m}\sqrt{\text{W}})$ , respectively, and  $|A_j|^2$  has unit of  $\text{W}$ . We note that such normalization is valid for any reciprocal waveguide structure, including waveguides with substantial loss. With such normalization, a wave in a single mode with unit amplitude (i.e.  $A_j(z) = 1$ ) carries a time-averaged power of  $c_j \text{W}$ , where

$$c_j = \int d\sigma \cdot \frac{1}{2} \text{Re}\{\mathbf{e}_{j,t} \times \mathbf{h}_{j,t}^*\}. \quad (3)$$

Notice that for lossless waveguides, one can show that both  $\mathbf{e}_{j,t}$  and  $\mathbf{h}_{j,t}$  can be taken to be real, and hence  $c_j = 1$ , reproducing the usual normalization condition [16]. Our normalization relation of Eq. (2), however, is more general, and is necessary for the lossy waveguide cases.

Following the derivation in the Appendix, in terms of the mode amplitudes  $A_j(z)$ , the coupled-mode equations that describe the DFG process in the waveguide are:

$$\begin{aligned}\frac{\partial A_1}{\partial z} &= -\frac{\alpha_1}{2} A_1 + \frac{i\omega_1}{4} \kappa_1 A_2^* A_3 \exp(i\Delta\beta z) \\ \frac{\partial A_2}{\partial z} &= -\frac{\alpha_2}{2} A_2 + \frac{i\omega_2}{4} \kappa_2 A_1^* A_3 \exp(i\Delta\beta z) \\ \frac{\partial A_3}{\partial z} &= -\frac{\alpha_3}{2} A_3 + \frac{i\omega_3}{4} \kappa_3 A_1 A_2 \exp(-i\Delta\beta z),\end{aligned}\quad (4)$$

where  $\alpha_j$  is the power propagation loss coefficient for the  $j$ -th mode,  $\Delta\beta \equiv \beta_3 - \beta_2 - \beta_1$ , and the coupling coefficients are

$$\begin{aligned}\kappa_1 &= \int d\sigma \bar{\chi} : \mathbf{e}_2^* \mathbf{e}_3 \cdot (\mathbf{e}_{1t} - \mathbf{e}_{1z}) \\ \kappa_2 &= \int d\sigma \bar{\chi} : \mathbf{e}_1^* \mathbf{e}_3 \cdot (\mathbf{e}_{2t} - \mathbf{e}_{2z}) \\ \kappa_3 &= \int d\sigma \bar{\chi} : \mathbf{e}_1 \mathbf{e}_2 \cdot (\mathbf{e}_{3t} - \mathbf{e}_{3z}).\end{aligned}\quad (5)$$

We note that the coupling coefficients have unit of  $s/(\text{m}\sqrt{\text{W}})$ . For a waveguide with length  $L$ , pumped by two optical beams with amplitudes  $A_2(0)$  and  $A_3(0)$  at  $z = 0$ , the conversion efficiency is:

$$\eta = \frac{P_1(L)}{P_2(0)P_3(0)} = \frac{c_1}{c_2 c_3} \left| \frac{A_1(L)}{A_2(0)A_3(0)} \right|^2$$

where  $P_1$  is the generated THz power and  $P_2$  and  $P_3$  are the pump powers. Under the approximation where the pump is not depleted by the nonlinear conversion process, one can solve Eq. (4) analytically to obtain the conversion efficiency:

$$\eta = \frac{c_1}{c_2 c_3} \frac{\omega_1^2 |\kappa_1|^2}{16} \left| \frac{\exp(\frac{\alpha_1 - \alpha_2 - \alpha_3}{2} L + i\Delta\beta L) - 1}{\frac{\alpha_1 - \alpha_2 - \alpha_3}{2} + i\Delta\beta} \right|^2 \exp(-\alpha_1 L) \quad (6)$$

Examining Eq. (6), we note several key factors that are important in order to achieve high conversion efficiency:

(a) Achieving large  $\kappa_1$ . To do so, from Eq. (5) we see that with respect to the modal profile, the orientation of the nonlinear crystal needs to be appropriately chosen. Moreover, since the amplitude of the electric field in a modal profile in general scales inversely with the modal size, as can be seen from the normalization relation of Eq. (2), tightly confining both the THz and the optical waves in the same waveguide structure is of great advantage.

(b) Phase matching. The conversion efficiency is typically maximized when the phase-matching condition is satisfied, i.e.  $\Delta\beta = 0$ . As an illustration, assuming that loss is zero, the efficiency  $\eta$  [Eq. (6)] is then proportional to  $L^2$ . Thus, one can achieve high conversion efficiency simply by increasing the length of the waveguide. Since  $\omega_1 = \omega_3 - \omega_2$ , the phase matching condition can equivalently be described as  $n_{THz} = n_g$ , where  $n_{THz} = c\beta_1/\omega_1$  is the phase index of the THz waves,  $n_g = c\frac{\beta_3 - \beta_2}{\omega_3 - \omega_2}$  is approximately the group index of the optical waves, and  $c$  is the speed of light in vacuum.

(c) Reducing propagation losses. Setting  $\Delta\beta = 0$  in Eq. (6) and solving  $d\eta/dL = 0$ , we obtain the optimal waveguide length which maximizes the conversion efficiency:

$$L_{\max} = \frac{2}{\alpha_1 - \alpha_2 - \alpha_3} \ln \left( \frac{\alpha_1}{\alpha_2 + \alpha_3} \right) \quad (7)$$

Thus, the presence of propagating losses limits the length of the waveguides that can be used for conversion purposes, even when phase-matching condition is satisfied.

### 3. An example of a high-efficiency waveguide device

Based on the theoretical condition presented above, we consider a waveguide geometry as shown in Fig. 1(a). The background material is quartz, and the silver film and the GaAs strip have the same thickness of  $h = 0.3 \mu\text{m}$ . The width of the slot and the GaAs strip are  $w_1 = 4 \mu\text{m}$  and  $w_2 = 0.24 \mu\text{m}$  respectively.

In choosing the background material, it is desirable that: (a) The background material has low loss in both the optical and THz wavelength; (b) Its index in the THz region is substantially

higher than in the optical region. Thus, quartz becomes an interesting choice. Other material can be used as background as well. From a loss perspective alone, an obvious choice of background material might have been air, provided that a long GaAs air bridge can be made (for an example of a GaAs air bridge, see [17]). In such a case, however, it turns out to be substantially more difficult to design the system for phase matching, while maintaining strong optical confinement in the GaAs region. Quasi-phase matching techniques [18], therefore, may be needed.

The focus of our paper is obviously theoretical with the aim to highlight the basic operating principles and considerations for this class of structures. Nevertheless, one could imagine a fabrication process, for the structure shown in Fig. 1, through a combination of wafer bonding [19, 20] and micro-manipulation techniques [21, 22]. The process consists of three steps: 1) A GaAs-on-quartz wafer is fabricated by the bonding technique, and then a GaAs strip is defined by etching the top GaAs layer; 2) Two metal regions and a void slot are fabricated on another quartz wafer by lithography; 3) The first wafer is mounted face-down on the second by the micro manipulation techniques.

The structure is designed to operate with two optical pump frequencies at 148.5 and 151.5 THz, respectively (the corresponding wavelengths are 2.02 and 1.98  $\mu\text{m}$ ). These two optical pumps will mix to generate a wave at 3THz. The refractive indices of all materials involved at these frequencies are summarized in Table 1.

Table 1. Refractive index ( $n$ ) of materials in the waveguide[23, 24, 25, 26]

Frequency (THz)	Ag	GaAs	Quartz (ordinary polarization)
3	$249.26 + i601.77$	$3.6 + i2.78 \times 10^{-3}$	$2.13 + i3.58 \times 10^{-4}$
148.5	$0.215 + i14.608$	3.341	1.522
151.5	$0.207 + i14.317$		

In the nonlinear conversion process, we assume that the two optical pumps have their electric fields predominantly along the  $y$  direction, and the THz wave has its electric field along the  $x$  direction. In order for these waves to interact, the orientation of GaAs is chosen such that a [011] direction coincides with the  $y$ -axis, and a [100] direction coincides with the  $x$ -axis [Fig. 1(b)]. As a result, the two optical pump beams can generate a polarization in THz along the  $x$ -axis through the  $d_{14}$  component in the  $\bar{\chi}^{(2)}$  tensor of GaAs. Here we use  $d_{14} = 46.1$  pm/V [27].

To calculate the conversion efficiency, we use a finite-difference frequency-domain (FDFD) code to calculate the wave number ( $\beta_j$ ), the loss coefficient ( $\alpha_j$ ), and the modal profile of all the relevant modes. To take into account the field penetration into the metal, a variable grid is used. For the THz wave, we use a computational window size of 200  $\mu\text{m}$  by 200  $\mu\text{m}$ , with a minimal grid spacing of 10 nm. For the optical wave, we use a computational window size of 20  $\mu\text{m}$  by 20  $\mu\text{m}$  with a minimal grid spacing of 5 nm. After obtaining the modal information, the nonlinear coupling coefficient  $\kappa_j$  is then calculated with Eq. (5). By numerically solving the nonlinear coupled-mode equations [Eq. (4)] (we assume that the two pumps have equal power), we obtain the THz output power and hence the conversion efficiency. Such a calculation does not assume the undepleted-pump approximation.

Figure 2(a) plots the THz output power versus the waveguide length for different pump powers. The conversion efficiency typically increases as a function of waveguide length, until the loss of the waveguide becomes substantial. At all pump powers, the maximum THz output occurs when the waveguide length is approximately 10 mm, as compared to  $L_{max} = 10.4$  mm calculated by Eq. (7) under the undepleted-pump approximation. Figure 2(b) shows the THz output power for a 10 mm long waveguide as a function of the pump power. The conversion efficiency is  $5.66 \times 10^{-6} \text{ W}^{-1}$ , as compared to  $\eta = 5.71 \times 10^{-6} \text{ W}^{-1}$  calculated by Eq. (6).

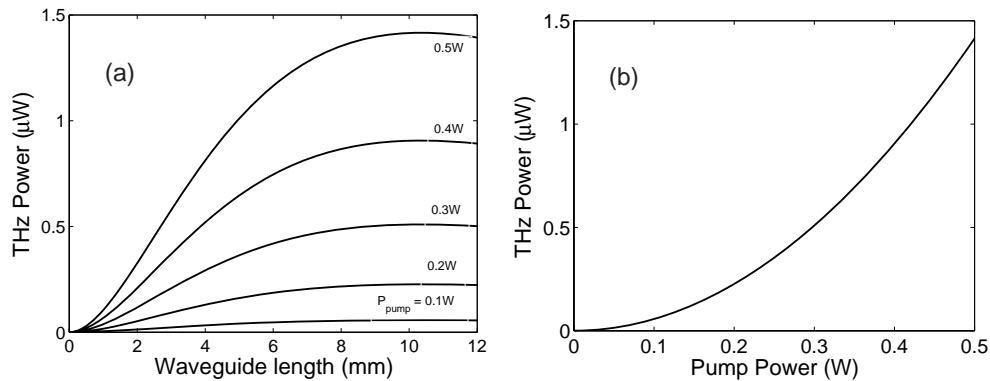


Fig. 2. (a) THz output power as a function of the waveguide length. Here we assume that the two optical pumps have equal power. (b) THz output power for the 10 mm long waveguide as a function of the pump power.

Thus, the full solution of the nonlinear ordinary differential equations of Eq. (4) indicates that the non-depleted pump approximation is generally valid in this system. The conversion efficiency is more than one order of magnitude larger than the highest previously reported for conventional dielectric waveguides [11].

#### 4. Discussion of the design requirement

We now discuss some detailed considerations that lead to the design in the previous section. The efficiency improvement in this geometry arises from the strong confinement of THz wave, enabled by the use of the metallic structures. However, the use of metallic structures also induces losses for both the optical and the THz waves. The structure shown in Fig. 1 is designed by considering this trade-off between confinement and propagation loss.

To discuss the design consideration, we first briefly discuss some of the relevant modal properties of the waveguide. This waveguide supports guided modes at both the THz and the optical frequency ranges. The corresponding dispersion relations and the modal profiles are shown in Figs. 3 and 4, respectively.

In the THz frequency range, the waveguide supports a single quasi-TEM mode with its electric field lines going from one metal region to the other [Fig. 4(a-b)]. Notice that the mode is mostly confined in the slot region. Thus, the mode has a transverse dimension of approximately  $8 \mu\text{m}$  that is much smaller than the  $100 \mu\text{m}$  free space wavelength of a 3 THz wave. Since the THz mode is a quasi-TEM mode, its dispersion relation is strongly influenced by the materials in the slot, which for our geometry is mostly filled with quartz. Our FDFD calculations show a  $n_{\text{THz}} \simeq 2.14$ , as compared to the refractive index of 2.13 for quartz at the same wavelength. In the THz wavelength range, there is typically substantial material loss due to phonon-polariton excitations. At 3 THz, the loss coefficient of quartz is approximately  $0.6 \text{ cm}^{-1}$ . The use of metal induces additional THz loss due to the finite penetration of fields into the metal. The penetration depth is approximately 50 nm. The FDFD calculations indicate that the THz mode has a loss coefficient  $\alpha_1 \simeq 4.59 \text{ cm}^{-1}$ . Thus, in this structure the loss at the THz wavelength range is dominated by metal loss.

The optical modes of this structure are largely guided by the GaAs strip and the modal profiles decay exponentially in quartz away from the GaAs strip [Fig. 4(c-d)]. In principle, to maximally confine an optical wave, one typically would choose the width of the strip to be about half a wavelength in the core material. However, maximizing the optical modal confine-

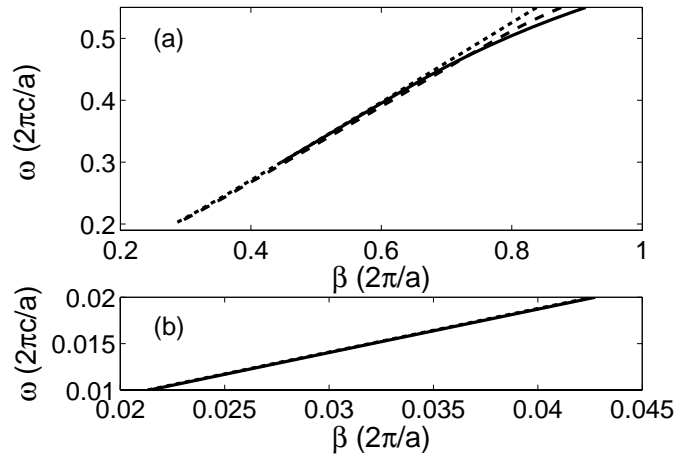


Fig. 3. Dispersion relation of the slot waveguide shown in Fig. 1. All frequencies are normalized with respect to a length scale of  $a = 1\mu\text{m}$ . (a) In the optical frequency range  $0.3 \sim 0.55$  ( $c/a$ ) (i.e.  $90 \sim 165$  THz), the waveguide supports two modes: The electric fields of these two modes are polarized predominantly along the  $y$  or  $x$ -axis. The dispersion relations of these two modes correspond to the solid and dashed line, respectively. The dotted line is the light line of quartz. (b) Dispersion relation of the slot waveguide in the THz range.

ment in GaAs also implies that the modal index is comparable to that of GaAs. On the other hand, to satisfy the phase matching condition the group index of the optical modes needs to be comparable to the THz refractive index of quartz. Thus, we have instead chosen the width and the thickness of GaAs strip to be  $w_2 = 0.24$  and  $h = 0.3 \mu\text{m}$  such that the optical mode substantially extends into quartz, which lowers the group index to  $n_g = 2.14$ , satisfying the phase matching constraint.

In the optical wavelength range, the linear loss of the dielectric material is typically negligible. The intrinsic loss mechanism in the dielectric is instead due mainly to two-photon absorption. With a choice of optical wavelength of  $2\mu\text{m}$ , the optical photon energy is below half of the band gap of GaAs [28], and the nonlinear loss can be ignored. As a result, the dielectrics can be treated as essentially lossless. In the optical frequency range, the modal loss is entirely due to the presence of metal. For the slot waveguide, increasing the width of the slot, such that eventually the optical modes do not extend into the metal region, is therefore effective in reducing the optical loss. Figure 5 shows the propagation loss at  $\omega_2$  as a function of slot width. As the slot width increases beyond  $4 \mu\text{m}$ , the loss of the optical modes drops below  $1\text{cm}^{-1}$ . For the slot width  $w_1 = 4 \mu\text{m}$ , the loss coefficients for the two pumps are  $\alpha_2 = 0.36 \text{cm}^{-1}$  and  $\alpha_3 = 0.20 \text{cm}^{-1}$ .

We note that, while increasing the slot width reduces the optical loss, it also reduces the modal overlap, and hence the nonlinear coupling coefficient  $\kappa$ . Figures 6(a-b) show the coupling coefficient and the maximum conversion efficiency, respectively, as a function of slot width. Without considering the phase mismatching induced by the slot width variation, i.e. by setting  $\Delta\beta = 0$  in the calculation, the conversion efficiency has a maximum value of  $7.1 \times 10^{-6} \text{W}^{-1}$  at  $w_1 = 6 \mu\text{m}$ . The use of a narrower slot leads to higher optical propagation loss, whereas the use of a wider slot reduces the coupling coefficient. Figure 6(b) also shows that the phase mismatching further reduces the conversion efficiency.

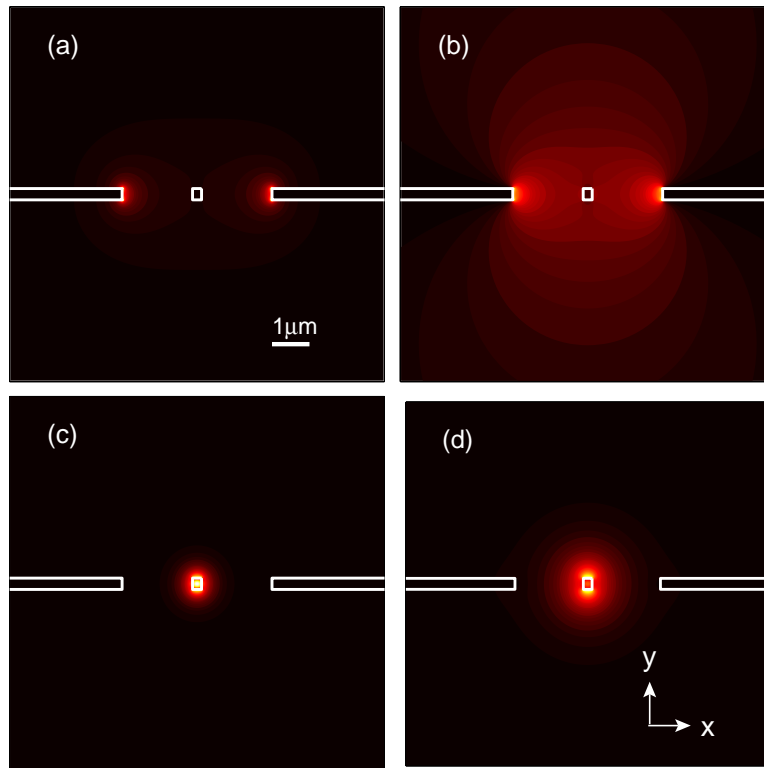


Fig. 4. (a) Power density profile and (b) the real part of  $E_x$  of the guided mode at the frequency  $f = 0.01(c/a) = 3$  THz in Fig. 3(b). (c) Power density profile and (d) the real part of  $E_y$  of the second waveguide mode [solid line in Fig. 3(a)] at  $f = 0.495(c/a) = 148.5$  THz. The white lines give the outline of the waveguide structure.

## 5. Design procedure for general pump wavelengths

The example presented above is for a specific set of pump wavelengths. Here we point out a design procedure for general pump wavelengths. An important feature, from the discussions above, is that the metal region needs to be placed sufficiently far away from the GaAs strip in order to reduce optical loss. Here, we show that this feature allows near-independent design of optical and THz modes for phase-matching purposes. As a result, we present a two-step process that allows design of slot waveguides for THz conversion process at general pump wavelengths. Because the method is based on the dispersion relation of guided modes, rather than the material dispersion, it can be applied to other material systems.

Let's first consider the optical mode. The optical modal fields exponentially decay along the transverse directions in the surrounding quartz region. Thus, when the slot is wide enough, the impact of the metallic structure on the optical mode dispersion relation is negligible. For example, the dispersion relation in a waveguide with a slot width  $w_1 = 3 \mu\text{m}$  almost coincides with that in a GaAs strip waveguide without the metal, as seen in Fig. 7. Thus, to design a waveguide with the correct optical mode index, it is sufficient to consider only the GaAs strip waveguide, which greatly reduces the dimensions of the parameter space and hence simplifies the design process.

We now consider the THz modes. In Fig. 8, we plot the effective index and the propaga-

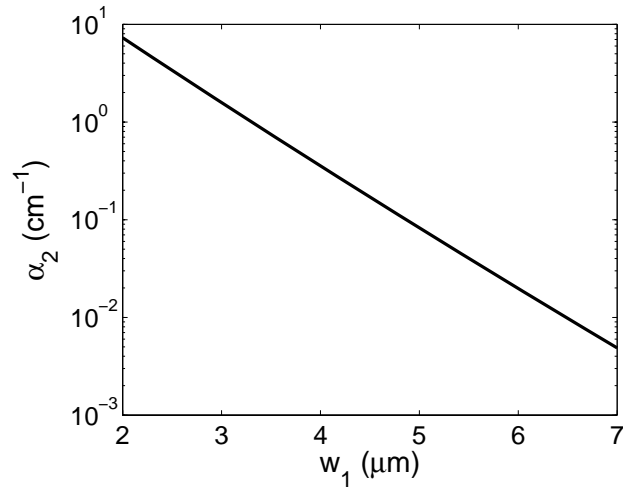


Fig. 5. Optical propagation loss at  $\omega_2$  as a function of slot width. Here the dimensions of the GaAs strip and the thickness of the metal film are fixed at  $w_2 = 0.24 \mu\text{m}$  and  $h = 0.3 \mu\text{m}$ .

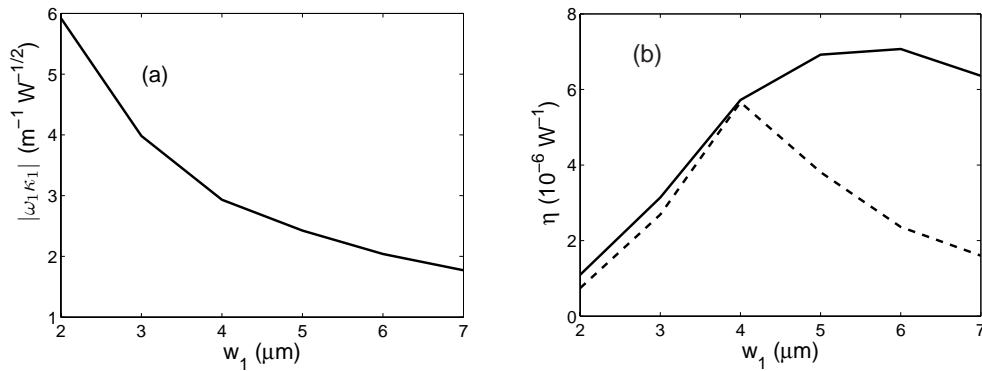


Fig. 6. (a) Coupling coefficient as a function of slot width. (b) Maximum conversion efficiency as a function of slot width. The other geometry parameters are fixed at  $w_2 = 0.24 \mu\text{m}$  and  $h = 0.3 \mu\text{m}$ , and the pump power is  $0.5 \text{ W}$ . The solid (dashed) line denotes the case without (with) considering the phase mismatching induced by the slot width variation.

tion loss for the mode at 3 THz as a function of the slot width. Both the effective index and the propagation loss decrease with the slot width. Because the quasi-TEM modes are strongly concentrated near the edges of the metal, the fraction of the modal power in the GaAs strip decreases as the slot width increases. Consequently, for slots with width wider than  $4 \mu\text{m}$ , which is the regime of interest due to the consideration of losses in the optical modes, the index of the THz mode is essentially that of quartz.

Based on the discussions above on the properties of optical and THz modes, here we propose a two-step method to realize phase matching for general pump wavelengths. We first design a GaAs strip. We choose the width and the height of the strip, i.e.  $w_2$  and  $h$ , such that the group index at the pump wavelength  $n'_g$  is approximately equal but slightly larger than the refractive index of quartz  $n_b$  at the THz wavelength range. We then consider a slot waveguide with such

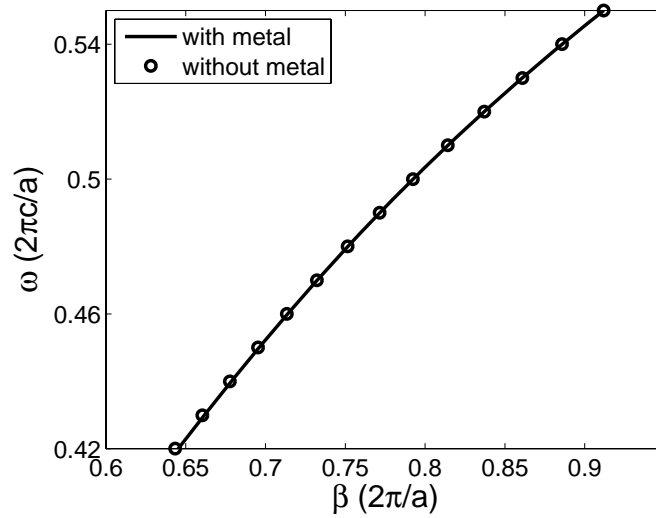


Fig. 7. Dispersion relations for two waveguides: (i) a waveguide as in Fig. 1 with slot width  $w_1 = 3 \mu\text{m}$  (solid line); (ii) a GaAs strip waveguide without metal slot structure (circles). In both cases, the dimensions of the GaAs strip are  $w_2 = 0.24 \mu\text{m}$  and  $h = 0.3 \mu\text{m}$ .

GaAs strip embedded in it. For simplicity, the thickness of the metal layer is chosen to be the same as that of the GaAs strip. Thus, we will be aiming to determine the width  $w_1$  of the slot. To do so, we first search for an initial value of  $w_1$ , such that the corresponding optical propagation loss is low, and the group index of the pumps  $n_g''$  and the effect index of the THz mode  $n_{THz}''$  are subject to  $n_g'' \approx n_g'$  and  $n_{THz}'' > n_g'$ ; then we gradually increase the slot width until the phase matching condition  $n_{THz}'' = n_g''$  is satisfied. This process allows to always find a width  $w_1$  since with increasing  $w_1$ ,  $n_g''$  is still roughly equal to  $n_g'$  while  $n_{THz}''$  monotonically decreases and approaches to  $n_b$  that is less than  $n_g'$ .

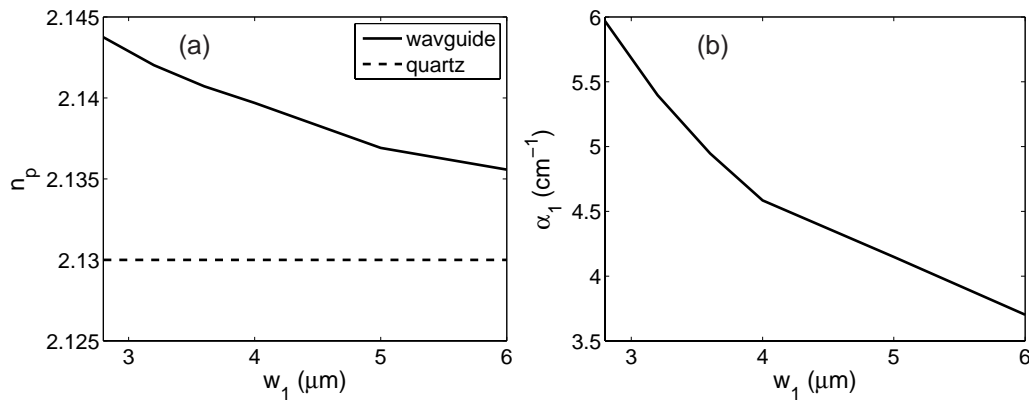


Fig. 8. (a) Effective index and (b) propagation loss for 3 THz guided modes as a function of  $w_1$ , where the other geometry parameters are fixed at  $w_2 = 0.4 \mu\text{m}$  and  $h = 0.3 \mu\text{m}$ .

## 6. Conclusion

In conclusion, we have investigated in detail a metallic slot waveguide, for the purpose of enhancing optics-to-THz conversion efficiency. To exactly describe the frequency conversion process in lossy waveguides, a coupled-mode theory with fully vectorial form is developed. Using the coupled-mode theory, we outline the basic theoretical requirements for efficient frequency conversion, which include the needs to achieve large coupling coefficients, phase matching, and low propagation loss for both the optical and THz waves. Following these requirements, a metallic waveguide is designed by considering the trade-off between modal confinement and propagation loss. Our numerical calculation shows that the conversion efficiency is more than one order of magnitude higher than what has been achieved using dielectric waveguides. Based on different behaviors of the optical and THz modal dispersion as a function of slot width, we propose a two-step method to realize the phase matching for general pump wavelengths.

This work is supported by AFOSR (Grant No. FA9550-1-04-0437).

### Appendix: Derivation of the coupled-mode equations for difference frequency generation in a lossy waveguide under nonlinear interaction

Here we derive the coupled-mode equations to describe nonlinear interaction of co-propagating waves in a waveguide. The derivation is based on the reciprocity theorem, which gives rise to an orthogonality theorem of guided modes. As a starting point, we briefly review these two theorems. Their detailed derivations can be found in Ref. [29].

*Reciprocity theorem for waveguides* - Consider two guided waves  $\{\mathbf{E}_i, \mathbf{H}_i\}$  ( $i = 1, 2$ ) in a  $z$ -invariant waveguide, each excited by a current density  $\mathbf{J}_i$ , respectively. From Maxwell's equations:

$$\begin{aligned}\nabla \times \mathbf{E}_1 &= i\omega\mu\mathbf{H}_1 \\ \nabla \times \mathbf{H}_1 &= -i\omega\varepsilon\mathbf{E}_1 + \mathbf{J}_1 \\ \nabla \times \mathbf{E}_2 &= i\omega\mu\mathbf{H}_2 \\ \nabla \times \mathbf{H}_2 &= -i\omega\varepsilon\mathbf{E}_2 + \mathbf{J}_2,\end{aligned}\quad (8)$$

and by further assuming that the current densities  $\mathbf{J}_i$  are continuously varying along  $z$ , we obtain the reciprocity theorem:

$$\int_S d\sigma \cdot \frac{\partial}{\partial z} (\mathbf{E}_1 \times \mathbf{H}_2 - \mathbf{E}_2 \times \mathbf{H}_1) = \int_S d\sigma (\mathbf{J}_1 \cdot \mathbf{E}_2 - \mathbf{J}_2 \cdot \mathbf{E}_1) \quad (9)$$

where  $S$  is any slice of the waveguide normal to  $z$ . Importantly, this theorem is valid for both lossless and lossy media, i.e. it applies to the case where  $\varepsilon$  is complex.

*Orthogonality theorem of guided modes* - We consider a source-free waveguide. Suppose  $\{\mathbf{E}_i, \mathbf{H}_i\}$  ( $i = 1, 2$ ) are two guided modes satisfying Eq. (8) with  $\mathbf{J}_1 = \mathbf{J}_2 = 0$ . Splitting each of these two modes into the transverse  $\{\mathbf{e}_{i,t}, \mathbf{h}_{i,t}\}$  and longitudinal parts  $\{\mathbf{e}_{i,z}, \mathbf{h}_{i,z}\}$ , we obtain

$$\begin{aligned}\mathbf{E}_1 &= (\mathbf{e}_{1t} + \mathbf{e}_{1z}) \exp(iq_1 z) \\ \mathbf{H}_1 &= (\mathbf{h}_{1t} + \mathbf{h}_{1z}) \exp(iq_1 z) \\ \mathbf{E}_2 &= (\mathbf{e}_{2t} + \mathbf{e}_{2z}) \exp(iq_2 z) \\ \mathbf{H}_2 &= (\mathbf{h}_{2t} + \mathbf{h}_{2z}) \exp(iq_2 z)\end{aligned}\quad (10)$$

where  $q_i$  are the corresponding propagation constants that in general can be complex. The orthogonality theorem states that, when  $q_1 \neq q_2$ , the transversal parts of the two modes satisfy the following condition [29]:

$$\int_S d\sigma \cdot (\mathbf{e}_{1t} \times \mathbf{h}_{2t}) = 0. \quad (11)$$

*Coupled-mode equations for the nonlinear interaction in waveguides* - We now consider a waveguide with a source current density  $\mathbf{J}_1 = -i\omega\mathbf{P}_1^{NL}$  that arises from the nonlinear interaction. Such a source generates a guided wave  $\{\mathbf{E}_1, \mathbf{H}_1\}$  propagating along the  $+z$  direction, which can be expanded in terms of all guided modes at the same frequency:

$$\begin{aligned}\mathbf{E}_1 &= \sum_l \tilde{A}_l(z) (\mathbf{e}_{l,t} + \mathbf{e}_{l,z}) \exp(iq_l z) \\ \mathbf{H}_1 &= \sum_l \tilde{A}_l(z) (\mathbf{h}_{l,t} + \mathbf{h}_{l,z}) \exp(iq_l z),\end{aligned}\quad (12)$$

where  $\{\mathbf{e}_{l,t(z)}, \mathbf{h}_{l,t(z)}\}$  is the transverse (longitudinal) component of each guided mode propagating along  $+z$  in the source-free case, and  $l$  is the index for each mode. For the  $L$ -th mode, applying the mirror symmetry operation of the waveguide about the plane normal to  $z$ , one can show that

$$\begin{aligned}\mathbf{E}_2 &= (\mathbf{e}_{L,t} - \mathbf{e}_{L,z}) \exp(-iq_L z) \\ \mathbf{H}_2 &= (-\mathbf{h}_{L,t} + \mathbf{h}_{L,z}) \exp(-iq_L z)\end{aligned}\quad (13)$$

is also a guided mode that propagates along  $-z$ .

By substituting  $\mathbf{J}_1 = -i\omega\mathbf{P}_1^{NL}$ ,  $\mathbf{J}_2 = 0$ , and Eqs. (12) and (13) into Eq. (9), we observe that on the left hand of Eq. (9), only the  $\mathbf{e}_{l,t} \times \mathbf{h}_{L,t} + \mathbf{e}_{L,t} \times \mathbf{h}_{l,t}$  term is along the  $z$ -direction, the other terms are perpendicular to  $z$ , and therefore it is the only non-vanishing term once the surface integral along  $z$  is performed. By further applying the orthogonality condition [Eq. (11)], we obtain

$$\frac{\partial \tilde{A}_L(z)}{\partial z} = \frac{i\omega \int_S d\sigma (\mathbf{P}_1^{(NL)} \cdot (\mathbf{e}_{L,t} - \mathbf{e}_{L,z}))}{\int_S d\sigma \mathbf{e}_{L,t} \times \mathbf{h}_{L,t}} \exp(-iq_L z) \quad (14)$$

We now specifically consider the DFG process in the present waveguide where two optical waves at frequencies  $\omega_2$  and  $\omega_3$ , mix to produce a THz beam at  $\omega_1 = \omega_3 - \omega_2$ . For each frequency  $\omega_j$ , the guided wave  $\{\mathbf{E}_j, \mathbf{H}_j\}$  propagating along  $+z$ , has the following form:

$$\begin{aligned}\mathbf{E}_j &= \tilde{A}_j(z) (\mathbf{e}_{j,t} + \mathbf{e}_{j,z}) \exp(iq_j z) \\ \mathbf{H}_j &= \tilde{A}_j(z) (\mathbf{h}_{j,t} + \mathbf{h}_{j,z}) \exp(iq_j z).\end{aligned}\quad (15)$$

Here  $q_j = \beta_j + i\frac{\alpha_j}{2}$  is the complex propagating constant,  $\alpha_j$  and  $\beta_j$ , which are both real and positive, are the power propagation loss coefficient and the wave number, respectively. The modal profile  $\{\mathbf{e}_{j,t(z)}, \mathbf{h}_{j,t(z)}\}$  satisfies the orthonormal relation of Eq. (2). Comparing Eq. (15) with Eq. (1), we have

$$A_j(z) = \tilde{A}_j(z) \exp(-\frac{\alpha_j}{2} z). \quad (16)$$

Also, the THz nonlinear polarization  $\mathbf{P}_1^{NL} = \bar{\chi} : \mathbf{E}_2^* \mathbf{E}_3$  at the frequency  $\omega_1$  can be written as

$$\mathbf{P}_1^{NL} = \tilde{A}_2^* \tilde{A}_3 \exp(-\frac{\alpha_3 + \alpha_2}{2} z) \exp(i(\beta_3 - \beta_2) z) \bar{\chi} : \mathbf{e}_2^* \mathbf{e}_3 \quad (17)$$

where  $\bar{\chi}$  is the second-order susceptibility tensor. By substituting Eqs. (2), (15), and (17) into Eq. (14), we have

$$\frac{\partial \tilde{A}_1}{\partial z} = \frac{i\omega_1}{4} \kappa_1 \tilde{A}_2^* \tilde{A}_3 \exp(-\frac{\alpha_3 + \alpha_2}{2} z + \frac{\alpha_1}{2} z) \exp(i\Delta\beta z). \quad (18)$$

Here  $\Delta\beta = \beta_3 - \beta_2 - \beta_1$ , and  $\kappa_1$  is the coupling coefficient

$$\kappa_1 = \int_S d\sigma \bar{\chi} : \mathbf{e}_2^* \mathbf{e}_3 \cdot (\mathbf{e}_{1t} - \mathbf{e}_{1z}). \quad (19)$$

By substituting Eq. (16) into Eq. (18), we finally obtain the coupled-mode equation for the amplitude of the THz wave

$$\frac{\partial A_1}{\partial z} = -\frac{\alpha_1}{2}A_1 + \frac{i\omega_1}{4}\kappa_1 A_2^* A_3 \exp(i\Delta\beta z) \quad (20)$$

The coupled mode equations for the optical wave can be derived similarly.